

Euclid in a Taxicab: Sparse Blind Deconvolution with Smoothed ℓ_1/ℓ_2 Regularization

Audrey Repetti*, Mai Quyen Pham*,[†], Laurent Duval[†]
 Émilie Chouzenoux*, and Jean-Christophe Pesquet*

Abstract

The ℓ_1/ℓ_2 ratio regularization function has shown good performance for retrieving sparse signals in a number of recent works, in the context of blind deconvolution. Indeed, it benefits from a scale invariance property much desirable in the blind context. However, the ℓ_1/ℓ_2 function raises some difficulties when solving the nonconvex and nonsmooth minimization problems resulting from the use of such a penalty term in current restoration methods. In this paper, we propose a new penalty based on a smooth approximation to the ℓ_1/ℓ_2 function. In addition, we develop a proximal-based algorithm to solve variational problems involving this function and we derive theoretical convergence results. We demonstrate the effectiveness of our method through a comparison with a recent alternating optimization strategy dealing with the exact ℓ_1/ℓ_2 term, on an application to seismic data blind deconvolution.

1 Introduction

Many experimental settings are modeled as inverse problems. They resort to estimating an unknown signal $\bar{x} \in \mathbb{R}^N$ from observations $y \in \mathbb{R}^N$, through the measurement process:

$$y = \bar{h} * \bar{x} + w, \quad (1)$$

an illustration of which is provided in Fig. 1. Here, $\bar{h} \in \mathbb{R}^S$ represents an impulse response (e.g. a linear sensor response or a “blur” convolutive point spread function), $*$ denotes a discrete-time convolution operator (with appropriate boundary processing), and $w \in \mathbb{R}^N$ is a realization of a random variable modeling an additive noise. Standard approaches, such as Wiener filtering and its statistical extensions [1], aim at minimizing criteria based on the squared Euclidean norm (ℓ_2^2). However, the use of the sole least squares data fidelity term is prone to noise sensitivity and the addition of an ℓ_2^2 regularization often leads to over-smoothed estimates. The deconvolution problem becomes blind, even more ill-posed, when the blur kernel \bar{h} is unknown, and needs to be estimated as well as the target signal. Applications include communications (equalization or channel estimation) [2], nondestructive testing [3], geophysics [4–6], image processing [7–9], medical imaging and remote sensing [10]. Blind deconvolution, being an underdetermined problem, often requires additional hypotheses. A usual approach seeks estimates $(\hat{x}, \hat{h}) \in \mathbb{R}^N \times \mathbb{R}^S$ of (\bar{x}, \bar{h}) as minimizers of the sum of a data fidelity term and additional regularization terms on the signal and on the blur kernel. Such regularization functions account for a priori

*Université Paris-Est, LIGM, CNRS-UMR 8049.

[†]IFP Energies nouvelles.

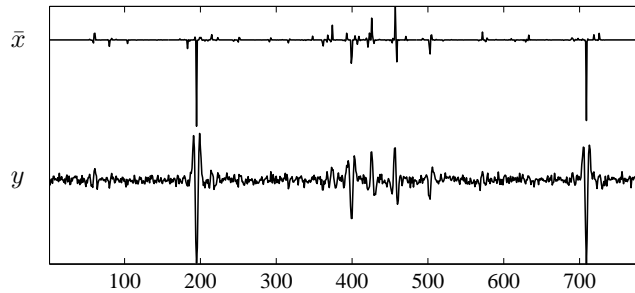


Figure 1: Unknown seismic signal \bar{x} (top), blurred/noisy observation y (bottom). assumptions one imposes on original sought objects, like sparsity, and ensure the stability of the solution. Blind deconvolution is subject to scaling ambiguity, and suggests scale-invariant contrast functions [11, 12].

A decade ago, a Taxicab-Euclidean norm ratio (ℓ_1/ℓ_2) arose as a sparseness measure [13–16], used in NMF (Nonlinear Matrix Factorization) [17]. Earlier mentions of a one-norm/two-norm ratio deconvolution appeared in geophysics [18]. It has since been used to constrain sharp images through wavelet frame coefficients [19], or for sparse recovery [20]. Such a regularization term is moreover suggested in [21] to avoid common pitfalls in blind sparse deconvolution.

Recently, [22] proposed an alternating minimization algorithm to deal with the ℓ_1/ℓ_2 regularization function. Its originality consists of transforming the ℓ_1/ℓ_2 nonconvex regularization term into a convex ℓ_1 regularization function. This is done in a reweighted fashion, by fixing the denominator ℓ_2 from the previous iterate. An iterative shrinkage-thresholding algorithm finally solves the remaining ℓ_1 regularized problem. Although the convergence of this approach has not been deeply investigated, it appears to be quite efficient in practice. More recently, [23] proposed a scaled gradient projection algorithm for minimizing a smooth approximation of the ℓ_1/ℓ_2 function, however limited to the case when the sparse signal to retrieve takes nonnegative values. We generalize this idea to a parametrized Smoothed One-Over-Two (SOOT) penalty for signed, real data. We present a novel efficient method based on recent results in nonconvex optimization combining an alternating minimization strategy with a forward-backward iteration [24, 25]. Moreover, we accelerate the convergence of our algorithm by using a Majorize-Minimize (MM) approach [25–27]. Section 2 introduces the minimization problem. Section 3 describes the proposed method and provides convergence results. The algorithm performance, compared with [22], is discussed in Section 4 for seismic data blind deconvolution. Some conclusions are drawn in Section 5.

2 Optimization model

2.1 Optimization tools

Our minimization strategy relies on two optimization principles. Let $U \in \mathbb{R}^{M \times M}$ be a symmetric positive definite (SPD) matrix. Firstly, we define the U -weighted proximity operator [28, Sec. XV.4], [29] of a proper, lower semicontinuous, convex function $\psi: \mathbb{R}^M \rightarrow]-\infty, +\infty]$ at $z \in \mathbb{R}^M$, relative to the metric induced by U , and denoted by $\text{prox}_{U,\psi}(z)$, as the unique minimizer of $\psi + \frac{1}{2}\|\cdot - z\|_U^2$, where $\|\cdot\|_U$ denotes the weighted Euclidean norm, i.e., $(\forall z \in \mathbb{R}^M) \|z\|_U = (z^\top U z)^{1/2}$. When U is equal to I_M , the identity matrix of $\mathbb{R}^{M \times M}$, then $\text{prox}_{I_M,\psi}$ reduces to the original definition of the proximity operator in [30]. We refer to [31–33] for additional details on proximity operators. Secondly, we introduce the Majoration-Minimization (MM) principle:

Definition 1. Let $\zeta: \mathbb{R}^M \rightarrow \mathbb{R}$ be a differentiable function. Let $z \in \mathbb{R}^M$. Let us define, for every $z' \in \mathbb{R}^M$,

$$q(z', z) = \zeta(z) + (z' - z)^\top \nabla \zeta(z) + \frac{1}{2} \|z' - z\|_{U(z)}^2,$$

where $U(z) \in \mathbb{R}^{M \times M}$ is a Semidefinite Positive (SDP) matrix. Then, $U(z)$ satisfies the majoration condition for ζ at z if $q(\cdot, z)$ is a quadratic majorant of the function ζ at z , i.e., for every $z' \in \mathbb{R}^M$, $\zeta(z') \leq q(z', z)$.

If function ζ has an L -Lipschitzian gradient on a convex subset $C \subset \mathbb{R}^M$, with $L > 0$, i.e., for every $(z, z') \in C^2$, $\|\nabla \zeta(z) - \nabla \zeta(z')\| \leq L \|z - z'\|$, then, for every $z \in C$, a quadratic majorant of ζ at z is trivially obtained by taking $U(z) = L I_M$.

2.2 Proposed criterion

From now on, definitions and properties apply for every $x = (x_n)_{1 \leq n \leq N} \in \mathbb{R}^N$ and $h \in \mathbb{R}^S$, unless otherwise stated. We propose to define an estimate (\hat{x}, \hat{h}) of (\bar{x}, \bar{h}) as a minimizer of the following penalized criterion:

$$F(x, h) = \rho(x, h) + g(x, h) + \varphi(x), \quad (2)$$

where $\rho(x, h) = \frac{1}{2} \|h * x - y\|^2$ is the least-squares objective function, g introduces additional a priori information on the sought objects, and φ models the One-Over-Two norm ratio non-convex penalty function [34], defined as the quotient of the following terms:

$$\ell_1(x) = \sum_{n=1}^N |x_n|, \quad \ell_2(x) = \left(\sum_{n=1}^N x_n^2 \right)^{1/2}. \quad (3)$$

The resulting regularization term is both nonconvex and nonsmooth, so that finding a minimizer of F is a challenging task.

We thus propose to replace the nonsmooth function ℓ_1/ℓ_2 by a maniable smooth approximation. More precisely, we employ the following surrogate function:

$$\varphi(x) = \lambda \log \left(\frac{\ell_{1,\alpha}(x) + \beta}{\ell_{2,\eta}(x)} \right), \quad (4)$$

with $(\lambda, \beta, \alpha, \eta) \in]0, +\infty[^4$.

The smooth approximations of ℓ_1 and ℓ_2 , $\ell_{1,\alpha}$ (sometimes called hybrid ℓ_1 - ℓ_2 or hyperbolic penalty) and $\ell_{2,\eta}$, are defined as follows with parametric constants (α, η) :

$$\ell_{1,\alpha}(x) = \sum_{n=1}^N \left(\sqrt{x_n^2 + \alpha^2} - \alpha \right), \quad \ell_{2,\eta}(x) = \sqrt{\sum_{n=1}^N x_n^2 + \eta^2}.$$

Note that ℓ_1 and ℓ_2 are recovered for $\alpha = \eta = 0$. The log function both makes the penalty easier to handle and, through its concavity, strengthens the flattening of the ℓ_1/ℓ_2 function toward sparsity. F corresponds to the Lagrangian function associated with the minimization of $\rho + g$ under the constraint

$$\log \left(\frac{\ell_{1,\alpha}(x) + \beta}{\ell_{2,\eta}(x)} \right) \leq \log(\vartheta), \quad (5)$$

for some positive constant ϑ . Owing to the monotonicity of the log function, (5) is equivalent to $(\ell_{1,\alpha}(x) + \beta)/\ell_{2,\eta}(x) \leq \vartheta$, which, according to (4), can be interpreted as a smooth approximation of an ℓ_1/ℓ_2 upper bound constraint, for β small enough. Finally, remark that lengthy but straightforward calculations allowed us to prove that φ has a Lipschitzian gradient on any bounded convex subset of \mathbb{R}^N , which is a desirable property for deriving an efficient algorithm to minimize (2). In the following, we assume that g can be split as

$$g(x, h) = g_1(x) + g_2(h), \quad (6)$$

where g_1 and g_2 are proper, lower semicontinuous, convex functions, continuous on their domain. Moreover, we denote by

$$f(x, h) = \rho(x, h) + \varphi(x), \quad (7)$$

the smooth part of the criterion, and $\nabla_1 f(x, h) \in \mathbb{R}^N$ (resp. $\nabla_2 f(x, h) \in \mathbb{R}^S$) the partial gradient of f with respect to the variable x (resp. h) computed at (x, h) .

3 Proposed alternating optimization method

3.1 Proposed SOOT algorithm

To minimize (2), one can exploit the block-variable structure of F by using an alternating forward-backward algorithm [24, 25, 35–37]. At each iteration $k \in \mathbb{N}$, this algorithm updates x^k (resp. h^k) with a gradient step on $f(\cdot, h^k)$ (resp. $f(x^k, \cdot)$) followed by a proximity step on g_1 (resp. g_2).

We use this alternating minimization method combined with an MM strategy, as described in [25]. For every $(x, h) \in \mathbb{R}^N \times \mathbb{R}^S$, let us assume the existence of SPD matrices $A_1(x, h) \in \mathbb{R}^{N \times N}$ and $A_2(x, h) \in \mathbb{R}^{S \times S}$ such that $A_1(x, h)$ (resp. $A_2(x, h)$) satisfies the majoration condition for $f(\cdot, h)$ at x (resp. $f(x, \cdot)$ at h). Then, the SOOT algorithm for the minimization of (2) is described in Algorithm 1. Note that PALM algorithm [24] is

Algorithm 1 SOOT algorithm.

For every $k \in \mathbb{N}$, let $J_k \in \mathbb{N}^*$, $I_k \in \mathbb{N}^*$ and let $(\gamma_x^{k,j})_{0 \leq j \leq J_k - 1}$ and $(\gamma_h^{k,i})_{0 \leq i \leq I_k - 1}$ be positive sequences. Initialize with $x^0 \in \text{dom } g_1$ and $h^0 \in \text{dom } g_2$.

Iterations:

For $k = 0, 1, \dots$

$$\left\{ \begin{array}{l} x^{k,0} = x^k, \quad h^{k,0} = h^k, \\ \text{For } j = 0, \dots, J_k - 1 \\ \quad \left\{ \begin{array}{l} \tilde{x}^{k,j} = x^{k,j} - \gamma_x^{k,j} A_1(x^{k,j}, h^k)^{-1} \nabla_1 f(x^{k,j}, h^k), \\ x^{k,j+1} = \text{prox}_{(\gamma_x^{k,j})^{-1} A_1(x^{k,j}, h^k), g_1}(\tilde{x}^{k,j}), \end{array} \right. \\ x^{k+1} = x^{k, J_k}. \\ \text{For } i = 0, \dots, I_k - 1 \\ \quad \left\{ \begin{array}{l} \tilde{h}^{k,i} = h^{k,i} - \gamma_h^{k,i} A_2(x^{k+1}, h^{k,i})^{-1} \nabla_2 f(x^{k+1}, h^{k,i}), \\ h^{k,i+1} = \text{prox}_{(\gamma_h^{k,i})^{-1} A_2(x^{k+1}, h^{k,i}), g_2}(\tilde{h}^{k,i}), \end{array} \right. \\ h^{k+1} = h^{k, I_k}. \end{array} \right.$$

recovered as a special case if $J_k \equiv I_k \equiv 1$ and, at each iteration, the Lipschitz constant of $\nabla_1 f(\cdot, h^k)$ (resp. $\nabla_2 f(x^{k+1}, \cdot)$) is substituted for $A_1(x^{k,0}, h^k)$ (resp. $A_2(x^{k+1}, h^{k,0})$). However, recent works on variable metric strategies [25, 27] show that the use of more

judicious preconditioning matrices can significantly accelerate the convergence of the algorithm. An example of such matrices is proposed in Section 3.2. Moreover, we show in our experimental part the practical interest in terms of convergence speed of taking the number of inner loops $(I_k)_{k \in \mathbb{N}}$ or $(J_k)_{k \in \mathbb{N}}$ greater than one.

The convergence of Algorithm 1 can be derived from the general results established in [25]:

Proposition 1. *Let $(x^k)_{k \in \mathbb{N}}$ and $(h^k)_{k \in \mathbb{N}}$ be sequences generated by Algorithm 1. Assume that:*

1. *There exists $(\underline{\nu}, \bar{\nu}) \in]0, +\infty[^2$ such that, for all $k \in \mathbb{N}$,*

$$\begin{aligned} (\forall j \in \{0, \dots, J_k - 1\}) \quad \underline{\nu} \mathbf{I}_N &\preceq A_1(x^{k,j}, h^k) \preceq \bar{\nu} \mathbf{I}_N, \\ (\forall i \in \{0, \dots, I_k - 1\}) \quad \underline{\nu} \mathbf{I}_S &\preceq A_2(x^{k+1}, h^{k,i}) \preceq \bar{\nu} \mathbf{I}_S. \end{aligned}$$

2. *Step-sizes $(\gamma_x^{k,j})_{k \in \mathbb{N}, 0 \leq j \leq J_k - 1}$ and $(\gamma_h^{k,i})_{k \in \mathbb{N}, 0 \leq i \leq I_k - 1}$ are chosen in the interval $[\underline{\gamma}, 2 - \bar{\gamma}]$ where $\underline{\gamma}$ and $\bar{\gamma}$ are some given positive real constants.*

3. *g is a semi-algebraic function.¹*

Then, the sequence $(x^k, h^k)_{k \in \mathbb{N}}$ converges to a critical point (\hat{x}, \hat{h}) of (2). Moreover, $(F(x^k, h^k))_{k \in \mathbb{N}}$ is a nonincreasing sequence converging to $F(\hat{x}, \hat{h})$.

3.2 Construction of the quadratic majorants

The numerical efficiency of the SOOT algorithm relies on the use of quadratic majorants providing tight approximations to the criterion and whose curvature matrices are simple to compute. The following proposition allows us to propose SDP matrices A_1 and A_2 for building majorizing approximations of f with respect to x and h .

Proposition 2. *For every $(x, h) \in \mathbb{R}^N \times \mathbb{R}^S$, let*

$$\begin{aligned} A_1(x, h) &= \left(L_1(h) + \frac{9\lambda}{8\eta^2} \right) \mathbf{I}_N + \frac{\lambda}{\ell_{1,\alpha}(x) + \beta} A_{\ell_{1,\alpha}}(x), \\ A_2(x, h) &= L_2(x) \mathbf{I}_S, \end{aligned}$$

where

$$A_{\ell_{1,\alpha}}(x) = \text{Diag} \left(\left((x_n^2 + \alpha^2)^{-1/2} \right)_{1 \leq n \leq N} \right), \quad (8)$$

and $L_1(h)$ (resp. $L_2(x)$) is a Lipschitz constant for $\nabla_1 \rho(\cdot, h)$ (resp. $\nabla_2 \rho(x, \cdot)$).² Then, $A_1(x, h)$ (resp. $A_2(x, h)$) satisfies the majoration condition for $f(\cdot, h)$ at x (resp. $f(x, \cdot)$ at h).

Proof. Let us decompose $\varphi = \varphi_1 + \varphi_2$ with $\varphi_1(x) = \lambda \log(\ell_{1,\alpha}(x) + \beta)$ and $\varphi_2(x) = -\lambda \log(\ell_{2,\eta}(x))$. It then suffices to prove that, for every $x \in \mathbb{R}^N$,

(i) $A_{\varphi_1}(x) = \frac{\lambda}{\ell_{1,\alpha}(x) + \beta} A_{\ell_{1,\alpha}}(x)$ satisfies the majoration condition for φ_1 at x ,

(ii) φ_2 has a μ -Lipschitzian gradient, with $\mu = \frac{9\lambda}{8\eta^2}$.

¹Semi-algebraicity is a property satisfied by a wide class of functions, which means that their graph is a finite union of sets defined by a finite number of polynomial inequalities. In particular, it is satisfied for the SOOT penalty, for standard numerical implementations of the log function.

²Such Lipschitz constants are straightforward to derive since ρ is a quadratic cost.

On the one hand, setting $\tau(x) = \ell_{1,\alpha}(x) + \beta$, we have [38]

$$\tau(x') \leq \tau(x) + (x' - x)^\top \nabla \tau(x) + \frac{1}{2} \|x' - x\|_{A_{\ell_{1,\alpha}}(x)}^2, \quad (9)$$

for every $x' \in \mathbb{R}^N$, where $A_{\ell_{1,\alpha}}(x)$ is given by (8).

On the other hand, for every $(u, v) \in]0, +\infty[^2$,

$$\log v \leq \log u + \frac{v}{u} - 1 = \log u + \frac{v - u}{u}. \quad (10)$$

By taking $v = \tau(x') > 0$ and $u = \tau(x) > 0$, and by combining (9) and (10), we obtain

$$\varphi_1(x') \leq \varphi_1(x) + \frac{\lambda}{\tau(x)} (x' - x)^\top \nabla \tau(x) + \frac{1}{2} (x' - x)^\top \frac{\lambda}{\tau(x)} A_{\ell_{1,\alpha}}(x) (x' - x).$$

Thus, Statement (i) is proved by remarking that $\nabla \varphi_1(x) = \frac{\lambda}{\tau(x)} \nabla \tau(x)$ and $A_{\varphi_1}(x) = \frac{\lambda}{\tau(x)} A_{\ell_{1,\alpha}}(x)$. On the other hand, the Hessian of φ_2 is given by

$$\nabla^2 \varphi_2(x) = \frac{2\lambda}{\ell_{2,\eta}^4(x)} x x^\top - \frac{\lambda}{\ell_{2,\eta}^2(x)} \mathbf{I}_N.$$

Noting that $\ell_{2,\eta}^2(x) = \|x\|^2 + \eta^2$, and applying the triangular inequality yield

$$\|\nabla^2 \varphi_2(x)\| \leq \frac{2\lambda \|x\|^2}{(\|x\|^2 + \eta^2)^2} + \frac{\lambda}{\|x\|^2 + \eta^2} = \chi(\|x\|),$$

where $\chi: u \in [0, +\infty[\mapsto \lambda \frac{3u^2 + \eta^2}{(u^2 + \eta^2)^2}$. The derivative of χ is given, for every $u \in [0, +\infty[$, by

$$\dot{\chi}(u) = \lambda \frac{2u}{(u^2 + \eta^2)^3} (\eta^2 - 3u^2),$$

thus χ is an increasing function on $[0, \eta/\sqrt{3}]$ and a decreasing function on $] \eta/\sqrt{3}, +\infty[$, and

$$\sup_{u \in [0, +\infty[} \chi(u) = \chi\left(\frac{\eta}{\sqrt{3}}\right) = \frac{9\lambda}{8\eta^2}.$$

Hence, the proof of Statement (ii). ■

4 Application to seismic data deconvolution

4.1 Problem statement

As some of the earliest mentions of ℓ_1/ℓ_2 deconvolution appeared in geophysics [18], blind seismic deconvolution (or inversion [39, 40]) is a natural application. The sparse seismic signal \bar{x} , of length $N = 784$, on the top of Fig. 1 is composed of a sequence of spikes termed primary reflection coefficients [41]. This reflectivity series indicates, in reflection seismology at normal incidence, the travel time of seismic waves between two seismic reflectors, and the amplitude of the seismic events reflected back to the sensor. The observed seismic trace y displayed in Fig. 1-bottom follows Model (1). In this context, the blur \bar{h} is related to the generated seismic source. We use here a band-pass ‘‘Ricker’’ seismic wavelet (or Mexican hat [42]) of size $S = 41$ (Fig. 3-bottom) with a frequency spectrum concentrated between 10 and 40 Hz. The additive noise w is a realization of a zero-mean white Gaussian noise with variance σ^2 . Since the reflectivity series is sparse, but limited in amplitude, we choose g_1 as the indicator function of the convex hypercube $[x_{\min}, x_{\max}]^N$. Similarly, as the seismic wavelet possesses finite energy, g_2 is equal to the indicator function of the set $\mathcal{C} = \{h \in [h_{\min}, h_{\max}]^S \mid \|h\| \leq \delta\}$, where $\delta > 0$, and h_{\min} (resp. h_{\max}) is the minimum (resp. maximum) value of \bar{h} .

4.2 Numerical results

Fig. 2 presents the variations of the reconstruction time, in seconds, with respect to the number of inner-loops $J_k \equiv J$, with $I_k \equiv 1$ and noise level $\sigma = 0.03$. The reconstruction time corresponds to the stopping criterion $\|x^k - x^{k-1}\| \leq \sqrt{N} \times 10^{-6}$. One can observe that the best compromise in terms of convergence speed is obtained for an intermediate number of inner-loops, namely $J = 71$. Note that the quality of the reconstruction is stable for each choice of J .

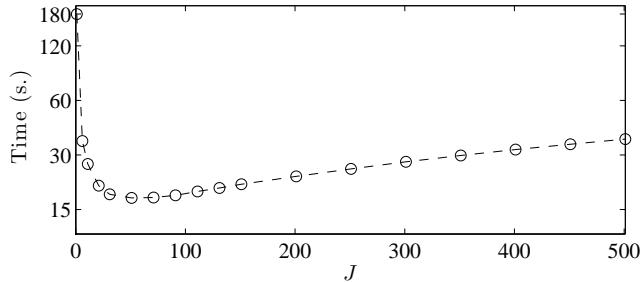


Figure 2: Reconstruction time for different numbers of inner-loops $J_k \equiv J$ (average over thirty noise realizations).

We gather comparisons of the SOOT algorithm³ with [22] in Table 1. Results presented in this table, for each noise level σ , are averaged over one hundred noise realizations. The regularization parameters of [22] and $(\lambda, \alpha, \beta, \eta) \in]0, +\infty[^4$ of (4) are adjusted so as to minimize the ℓ_1 norm between the original and the reconstructed signals. We also set, for every $k \in \mathbb{N}$, $J_k = 71$ and $I_k = 1$. If both methods yield tremendous improvements in ℓ_2 and ℓ_1 norms, the SOOT algorithm exhibits better results, for all noise levels, for both \bar{x} and \bar{h} estimates, especially in terms of ℓ_1 norm. Interestingly, the SOOT algorithm is also significantly faster in this application.

The performance is further assessed by subjective results for $\sigma = 0.03$. Fig. 3-top shows the residual error of the sparse signal estimation $\bar{x} - \hat{x}$, for a given noise realization, where \hat{x} is estimated with [22] in (a), and with SOOT in (b). It appears, in this example, that the error is smaller using SOOT algorithm. The estimated blur kernels look similar for both methods, as displayed in Fig. 3-bottom.

Noise level (σ)		0.01	0.02	0.03	
Observation error	$\ell_2 (\times 10^{-2})$	7.14	7.34	7.66	
	$\ell_1 (\times 10^{-2})$	2.85	3.44	4.08	
Signal error	[22]	$\ell_2 (\times 10^{-2})$	1.23	1.69	1.87
		$\ell_1 (\times 10^{-3})$	3.80	4.70	5.33
	SOOT	$\ell_2 (\times 10^{-2})$	1.22	1.63	1.85
		$\ell_1 (\times 10^{-3})$	3.43	4.30	4.86
Kernel error	[22]	$\ell_2 (\times 10^{-2})$	1.91	2.71	3.38
		$\ell_1 (\times 10^{-2})$	1.45	2.01	2.58
	SOOT	$\ell_2 (\times 10^{-2})$	1.69	2.27	2.98
		$\ell_1 (\times 10^{-2})$	1.25	1.76	2.33
Time (s.)	[22]	106	63	55	
	SOOT	39	26	18	

Table 1: Comparison between [22] and SOOT for \bar{x} and \bar{h} estimates (Intel(R) Xeon(R) CPU E5-2609 v2@2.5GHz using Matlab 8).

³The code will be made available at <http://www-syscom.univ-mlv.fr/> upon the paper acceptance.

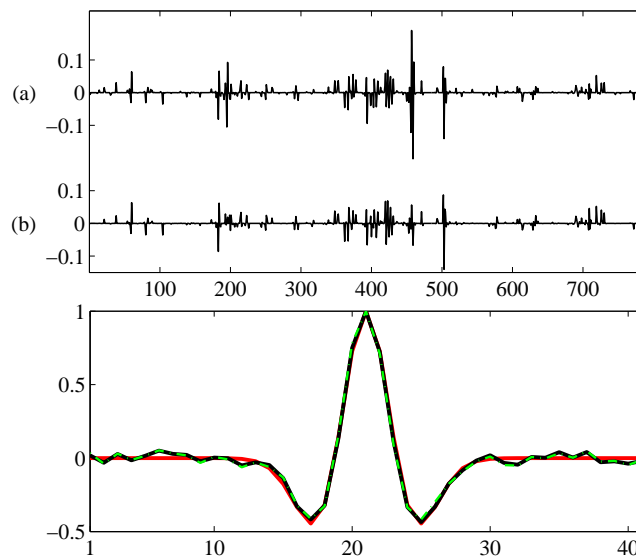


Figure 3: Top: signal estimation error $\bar{x} - \hat{x}$ with estimates \hat{x} given by [22] (a) and SOOT (b). Bottom: Original blur \bar{h} (continuous red), estimated \hat{h} with SOOT (continuous black) and [22] (dash-dotted green).

5 Conclusion

The proposed SOOT for minimizing an ℓ_1/ℓ_2 penalized criterion has been demonstrated to be quite effective in a blind deconvolution application on seismic reflectivity data. In addition, one of its advantages is that it offers theoretically guaranteed convergence. In future works, its use could be investigated for a broader class of application areas, where norm ratios are beneficial: adaptive filtering [43], compression [44], sparse system identification [45], sparse recovery [20], or cardinality-penalized clustering [46].

References

- [1] J.-C. Pesquet, A. Benazza-Benyahia, and C. Chaux, “A SURE approach for digital signal/image deconvolution problems,” *IEEE Trans. Signal Process.*, vol. 57, no. 12, pp. 4616–4632, Dec. 2009.
- [2] S. Haykin, Ed., *Blind Deconvolution*, Prentice Hall, 1994.
- [3] A. K. Nandi, D. Mampel, and B. Roscher, “Blind deconvolution of ultrasonic signals in nondestructive testing applications,” *IEEE Trans. Signal Process.*, vol. 45, no. 5, pp. 1382–1390, 1997.
- [4] K. F. Kaaresen and T. Taxt, “Multichannel blind deconvolution of seismic signals,” *Geophysics*, vol. 63, no. 6, pp. 2093–2107, Nov. 1998.
- [5] A. K. Takahata, E. Z. Nadalin, R. Ferrari, L. T. Duarte, R. Suyama, R. R. Lopes, J. M. T. Romano, and M. Tygel, “Unsupervised processing of geophysical signals: A review of some key aspects of blind deconvolution and blind source separation,” *IEEE Signal Process. Mag.*, vol. 29, no. 4, pp. 27–35, Jul. 2012.

- [6] M. Q. Pham, L. Duval, C. Chaux, and J.-C. Pesquet, “A primal-dual proximal algorithm for sparse template-based adaptive filtering: Application to seismic multiple removal,” *IEEE Trans. Signal Process.*, vol. 62, no. 16, pp. 4256–4269, Aug. 2014.
- [7] D. Kundur and D. Hatzinakos, “Blind image deconvolution,” *IEEE Signal Process. Mag.*, vol. 13, no. 3, pp. 43–64, May 1996.
- [8] D. Kundur and D. Hatzinakos, “Blind image deconvolution revisited,” *IEEE Signal Process. Mag.*, vol. 13, no. 6, pp. 61–63, Nov. 1996.
- [9] M. Kato, I. Yamada, and K. Sakaniwa, “A set-theoretic blind image deconvolution based on hybrid steepest descent method,” *IEICE Trans. Fund. Electron. Comm. Comput. Sci.*, vol. E82-A, no. 8, pp. 1443–1449, Aug. 1999.
- [10] P. Campisi and K. Egiazarian, Eds., *Blind Image Deconvolution: Theory and Applications*, CRC Press, 2007.
- [11] P. Comon, “Contrasts for multichannel blind deconvolution,” *Signal Process. Lett.*, vol. 3, no. 7, pp. 209–211, Jul. 1996.
- [12] É. Moreau and J.-C. Pesquet, “Generalized contrasts for multichannel blind deconvolution of linear systems,” *Signal Process. Lett.*, vol. 4, no. 6, pp. 182–183, Jun. 1997.
- [13] M. Zibulevsky and B. A. Pearlmutter, “Blind source separation by sparse decomposition in a signal dictionary,” *Neural Comput.*, vol. 13, no. 4, pp. 863–882, Apr. 2001.
- [14] P. Hoyer, “Non-negative matrix factorization with sparseness constraints,” *J. Mach. Learn. Res.*, vol. 5, pp. 1457–1469, 2004.
- [15] N. Hurley and S. Rickard, “Comparing measures of sparsity,” *IEEE Trans. Inf. Theory*, vol. 55, no. 10, pp. 4723–4741, Oct. 2009.
- [16] B. Barak, J. Kelner, and D. Steurer, “Rounding sum-of-squares relaxations,” Tech. Rep., Dec. 2013, <http://arxiv.org/abs/1312.6652>.
- [17] M. Mørup, K. H. Madsen, and L. K. Hansen, “Approximate L_0 constrained non-negative matrix and tensor factorization,” in *Proc. Int. Symp. Circuits Syst.*, May 2008, pp. 1328–1331.
- [18] W. C. Gray, “Variable norm deconvolution,” Tech. Rep. SEP-14, Stanford Exploration Project, Apr. 1978, http://sepwww.stanford.edu/oldreports/sep14/14_19.pdf.
- [19] H. Ji, J. Li, Z. Shen, and K. Wang, “Image deconvolution using a characterization of sharp images in wavelet domain,” *Appl. Comp. Harm. Analysis*, vol. 32, no. 2, pp. 295–304, 2012.
- [20] L. Demanet and P. Hand, “Scaling law for recovering the sparsest element in a subspace,” Tech. Rep., May 2014, <http://math.mit.edu/icg/papers/sparsest-element.pdf>.
- [21] A. Benichoux, E. Vincent, and R. Gribonval, “A fundamental pitfall in blind deconvolution with sparse and shift-invariant priors,” in *Proc. Int. Conf. Acoust. Speech Signal Process.*, Vancouver, Canada, May 26–31, 2013.

- [22] D. Krishnan, T. Tay, and R. Fergus, “Blind deconvolution using a normalized sparsity measure,” in *Proc. IEEE Conf. Comput. Vis. Pattern Recogn.*, Jun. 2011, pp. 233–240.
- [23] E. Esser, Y. Lou, and J. Xin, “A method for finding structured sparse solutions to non-negative least squares problems with applications,” *SIAM J. Imaging Sci.*, vol. 6, no. 4, pp. 2010–2046, 2013.
- [24] J. Bolte, S. Sabach, and M. Teboulle, “Proximal alternating linearized minimization for nonconvex and nonsmooth problems,” *Math. Progr. (Ser. A)*, Jul. 2013.
- [25] E. Chouzenoux, J.-C. Pesquet, and A. Repetti, “A block coordinate variable metric forward-backward algorithm,” Tech. Rep., 2013, http://www.optimization-online.org/DB_HTML/2013/12/4178.html.
- [26] S. Sotthivirat and J. A. Fessler, “Image recovery using partitioned-separable paraboloidal surrogate coordinate ascent algorithms,” *IEEE Trans. Image Process.*, vol. 11, no. 3, pp. 306–317, Mar. 2002.
- [27] E. Chouzenoux, J.-C. Pesquet, and A. Repetti, “Variable metric forward-backward algorithm for minimizing the sum of a differentiable function and a convex function,” *J. Optim. Theory Appl.*, vol. 162, no. 1, pp. 107–132, Jul. 2014.
- [28] J.-B. Hiriart-Urruty and C. Lemaréchal, *Convex Analysis and Minimization Algorithms*, Springer-Verlag, 1993.
- [29] P. L. Combettes and B. C. Vũ, “Variable metric quasi-Fejér monotonicity,” *Nonlinear Anal.*, vol. 78, pp. 17–31, Feb. 2013.
- [30] J. J. Moreau, “Proximité et dualité dans un espace hilbertien,” *Bull. Soc. Math. France*, vol. 93, pp. 273–299, 1965.
- [31] C. Chaux, P. L. Combettes, J.-C. Pesquet, and V. R. Wajs, “A variational formulation for frame based inverse problems,” *Inverse Probl.*, vol. 23, no. 4, pp. 1495–1518, Aug. 2007.
- [32] N. Pustelnik, C. Chaux, and J.-C. Pesquet, “Parallel proximal algorithm for image restoration using hybrid regularization,” *IEEE Trans. Image Process.*, vol. 20, no. 9, pp. 2450–2462, Sep. 2011.
- [33] P. L. Combettes and J.-C. Pesquet, “Proximal splitting methods in signal processing,” in *Fixed-point algorithms for inverse problems in science and engineering*, H. H. Bauschke, R. Burachik, P. L. Combettes, V. Elser, D. R. Luke, and H. Wolkowicz, Eds., pp. 185–212. Springer Verlag, 2011.
- [34] K. Slavakis, Y. Kopsinis, S. Theodoridis, and S. McLaughlin, “Generalized thresholding and online sparsity-aware learning in a union of subspaces,” *IEEE Trans. Signal Process.*, vol. 61, no. 15, pp. 3760–3773, Aug. 2013.
- [35] Z. Q. Luo and P. Tseng, “On the convergence of the coordinate descent method for convex differentiable minimization,” *J. Optim. Theory Appl.*, vol. 72, no. 1, pp. 7–35, Jan. 1992.

- [36] J. Bolte, P. L. Combettes, and J.-C. Pesquet, “Alternating proximal algorithm for blind image recovery,” in *Proc. Int. Conf. Image Process.*, Hong-Kong, China, Sep. 26-29, 2010, pp. 1673–1676.
- [37] Y. Xu and W. Yin, “A block coordinate descent method for regularized multiconvex optimization with applications to nonnegative tensor factorization and completion,” *SIAM J. Imaging Sci.*, vol. 6, no. 3, pp. 1758–1789, 2013.
- [38] M. Allain, J. Idier, and Y. Goussard, “On global and local convergence of half-quadratic algorithms,” *IEEE Trans. Image Process.*, vol. 15, no. 5, pp. 1130–1142, May 2006.
- [39] O. S. Osman and E. A. Robinson, Eds., *Seismic Source Signature Estimation and Measurement*, Number 18 in Geophysics Reprint Series. Soc. Expl. Geophysicists, Tulsa, OK, USA, 1996.
- [40] T. Ulrych and M. D. Sacchi, *Information-based inversion and processing with applications*, Elsevier, 2005.
- [41] A. T. Walden and J. W. J. Hosken, “The nature of the non-Gaussianity of primary reflection coefficients and its significance for deconvolution,” *Geophys. Prospect.*, vol. 34, no. 7, pp. 1038–1066, 1986.
- [42] N. Ricker, “The form and nature of seismic waves and the structure of seismograms,” *Geophysics*, vol. 5, no. 4, pp. 348–366, 1940.
- [43] P. Loganathan, A. W. H. Khong, and P. A. Naylor, “A class of sparseness-controlled algorithms for echo cancellation,” *IEEE Trans. Audio Speech Lang. Process.*, vol. 17, no. 8, pp. 1591–1601, Nov. 2009.
- [44] T. Drugman, “Maximum phase modeling for sparse linear prediction of speech,” *Signal Process. Lett.*, vol. 21, no. 2, pp. 185–189, Feb. 2014.
- [45] M. Yukawa, Y. Tawara, S. Sasaki, and I. Yamada, “A sparsity-based design of regularization parameter for adaptive proximal forward-backward splitting algorithm,” in *Proc. Int. Symp. Wireless Comm. Syst.*, Ilmenau, Germany, Aug. 27-30, 2013, pp. 1–4.
- [46] X. Chang, Y. Wang, R. Li, and Z. Xu, “Sparse K-means with ℓ_∞/ℓ_0 penalty for high-dimensional data clustering,” Tech. Rep., Mar. 2014, <http://arxiv.org/abs/1403.7890>.